DOI: 10.1002/ejic.201100192

Atomic Layer Deposition of Organic–Inorganic Hybrid Materials Based on Unsaturated Linear Carboxylic Acids

Karina B. Klepper,*[a] Ola Nilsen,[a] Thomas Levy,[a] and Helmer Fjellvåg[a]

Keywords: Organic–inorganic hybrid materials / Atomic layer deposition / Carboxylic acids / IR spectroscopy

The atomic layer deposition (ALD) technique has been further developed as a tool for producing thin films of organic–inorganic hybrid materials. Trimethylaluminium (TMA) and unsaturated linear carboxylic acids such as maleic acid, fumaric acid and *trans*,*trans*-muconic acid have been used as precursors, providing the possibility of also exploring the possible effect of *cis*- and *trans* configurations of the precursors. Quartz crystal microbalance measurements of the growth dynamics indicate that all systems are of a self-limiting ALD-type. Nevertheless, temperature-dependent growth, with decreasing growth rates with increasing deposition temperature, was observed. Growth rates were found to be in the range 0.24–1.19 nm/cycle. FTIR spectroscopy proved that the deposited films have a hybrid character. The carboxylic acids formed either bidentate or bridging complexes, and the *cis*- and *trans* configuration of the precursor influenced the preference for the type of bonding to the cation. All films were X-ray amorphous as deposited. The films were further analyzed by atomic force microscopy to determine the surface roughness and topography, UV/Vis spectroscopy and ellipsometry to evaluate the optical properties, and the goniometer method was employed to measure sessile drops for the surface wetting properties. All films are stable in contact with water. The films are generally smooth, transparent and have a refractive index in the range 1.5–1.6. Although the obtained films are dense when compared to attractive porous metal–organic framework (MOF) bulk materials, the present work shows that controlled growth of functionalized hybrid materials is offered by the ALD technique.

Introduction

Metal–organic framework structures (MOFs) have been studied intensively over the last decade and are a topic of major interest,[1] in particular, with respect to porous MOFs. However, very few of these materials have, until now, been produced as thin films.[2] Traditionally, the atomic layer deposition (ALD) technique has been used for the deposition of metals and inorganic compounds such as oxides, nitrides, sulfides etc.[3] Its excellent capabilities with respect to accurate control of growth, complete coverage, as well as a wide range of potential precursors incorporating most of the elements, provide an interesting basis for developing organic–inorganic hybrid materials with potential applications in devices and products. The deposition of such thin films by ALD, including surface-functionalized hybrid materials, has already been proven to be feasible. However, to date, the thin films are at best described as resembling metal–organic framework structures.

Here, we have restricted the term hybrid materials to cover combinations of organic- and inorganic components, where a direct reaction has taken place between these components, thus providing a mixture/network at the molecular level. Given this rather narrow operative definition, there nevertheless exists a large amount of published research in this area. Silicon-based structures have been the most widely studied so far.[4] Thin films of organic–inorganic hybrid materials containing elements other than silicon have previously been deposited by methods like Langmuir–Blodgett,[5] atomic layer deposition/molecular layer deposition (ALD/MLD),[6] single-source thermal ablation,[7] and sol–gel methods like spray-coating,[8] spin-coating,[9] and dip-coating.[10]

Organic–inorganic hybrid materials have various possibilities for multifunctionality that already have resulted in numerous applications as well as in important developments in fields like optical devices,[9a,9g,11] photoluminescence,[8–9,9e] protective coatings,[12] catalysis,[13] sensors,[4i,14] optoelectronic devices,[4d,4g,4k,9d,9g,10c,15] field-effect transistors,[4h,7a,7b,9d,9f] electroluminescence,[9b] light-emitting diodes,[7a] etc.

Silicon-based MOF materials have previously been used to control the wetting and friction properties of surfaces.[4e] Organic–inorganic hybrid thin films deposited by ALD have previously proven to generally be very smooth, gradient free, water resistant, and with a somewhat hydrophobic nature.[6c,6j] These material properties, in combination with the conformality offered by the ALD technique, may lead to new applications within tribology and for protective coatings.

[a] Department of Chemistry and Centre for Materials Science and Nanotechnology, University of Oslo,
P.O. Box 1033, Blindern, Oslo N-0315, Norway
Fax: +47-22-855-565
E-mail: k.b.klepper@kjemi.uio.no

Organic–inorganic hybrid materials may be envisaged as having higher elasticity than oxides and have therefore been suggested as diffusion barrier materials for flexible electronics.[6p,16] The growth rates of organic–inorganic hybrid materials by ALD are generally rather high when compared to their corresponding oxide, which enables efficient deposition of thicker films. Furthermore, they generally do not absorb UV/Vis light and have low refractive indices.[6a,6j] They may therefore be applied as low-index materials in optical coatings. The majority of MOF materials are dielectrics, which, when combined with the many possibilities with functionalization of the organic linkers, allows for the preparation of materials with highly tuneable dielectric properties.

The current contribution aims to expand further the field of organic–inorganic hybrid materials by reporting on the deposition of thin films with trimethylaluminium (TMA) and various unsaturated, linear carboxylic acids as building blocks. This thereby further extends the recently demonstrated depositions of hybrid materials based on carboxylic acids.[6c,6j] Previously, a similar type of growth has been demonstrated based on alcohols in the production of alucones by molecular layer deposition (MLD), in either a two-step or a three-step process, with TMA and ethylene glycol or TMA and ethanolamine and maleic anhydride, respectively.[6a,6b,6k,6p] TMA has also been used for the deposition of alkylsiloxane self-assembled multilayers (SAMs) by MLD, where the surface terminating functional groups were converted into carboxylic acid groups at an intermediate stage of the process.[4h] The present work is a contribution towards the development and study of novel types of materials that have general potential for a multitude of applications.

Results and Discussion

In situ quartz crystal microbalance (QCM) measurements were performed in order to extract pulse and purge parameters for each of the studied systems incorporating TMA and unsaturated linear carboxylic acids. This analysis relies on the Sauerbrey equation,[17] which states a linear dependency between the change in resonance frequency of the crystal and the mass of the deposited material. All systems exhibit signs of self-limiting growth, as illustrated in Figure 1.

The growth parameters, as extracted from Figure 1, and adopted sublimation temperatures for the organic precursors are given in Table 1.

The growth rates of the different systems were investigated as a function of deposition temperature (Figure 2) with the pulsing schemes presented in Table 1. All systems exhibit reasonably large ALD windows. However, the growth rate is dependent on the deposition temperature, even though the data from the QCM measurements were consistent with self-limiting growth. This is typical for non-ideal ALD growth windows, as described in ref.[3b]

The variations in density as a function of deposition temperature were calculated based on X-ray reflectometry (XRR) measurements (Figure 3). It should be noted that the density measurements performed by XRR are associated with uncertainties due to the sensitivity of the method towards sample alignment.

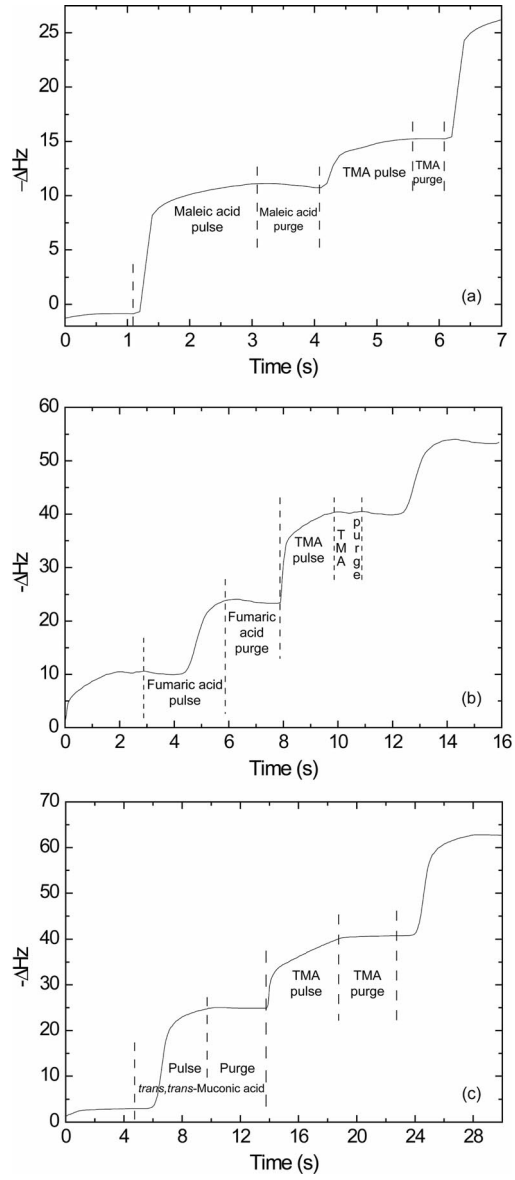

Figure 1. Changes in resonance frequency of a quartz microbalance as a function of film deposition with TMA and (a) maleic acid (at 186 °C), (b) fumaric acid (at 200 °C), and (c) *trans*,*trans*-muconic acid (at 250 °C).

Table 1. Parameters for the deposition of organic–inorganic hybrid materials.

	Pulse/Purge [s]	Pulse/Purge, TMA [s]	$T_{precursor}$ [°C]
Maleic acid (Fluka, ≥99.0%)	2.5/0.5	1.5/0.5	130
Fumaric acid (Fluka, ≥99.5%)	2.5/2.5	0.3/1.5	150
trans,*trans*-Muconic acid (Fluka, ≥97.0%)	3/2	0.5/2	200

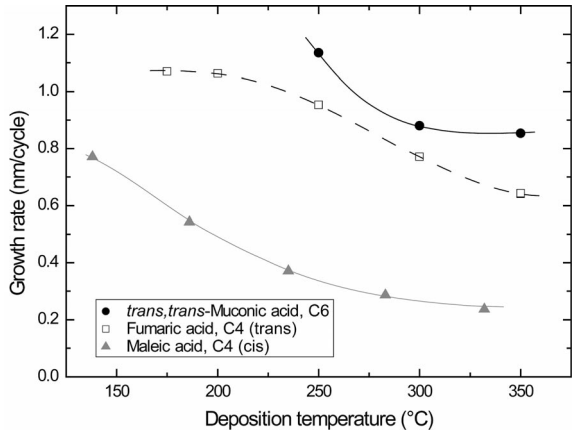

Figure 2. Film growth rates as a function of deposition temperature for the maleic acid/TMA, fumaric acid/TMA and *trans,trans*-muconic acid/TMA systems.

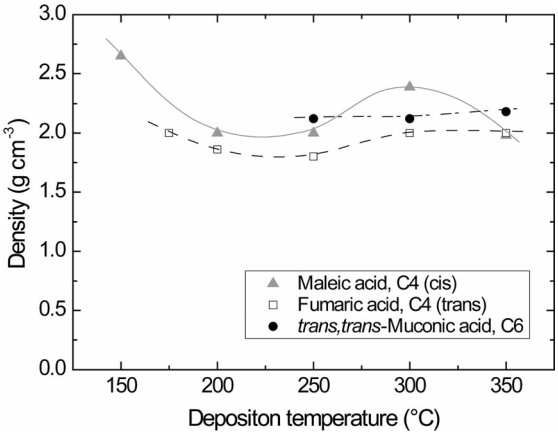

Figure 3. Film density as a function of deposition temperature for the carboxylic acid/TMA systems.

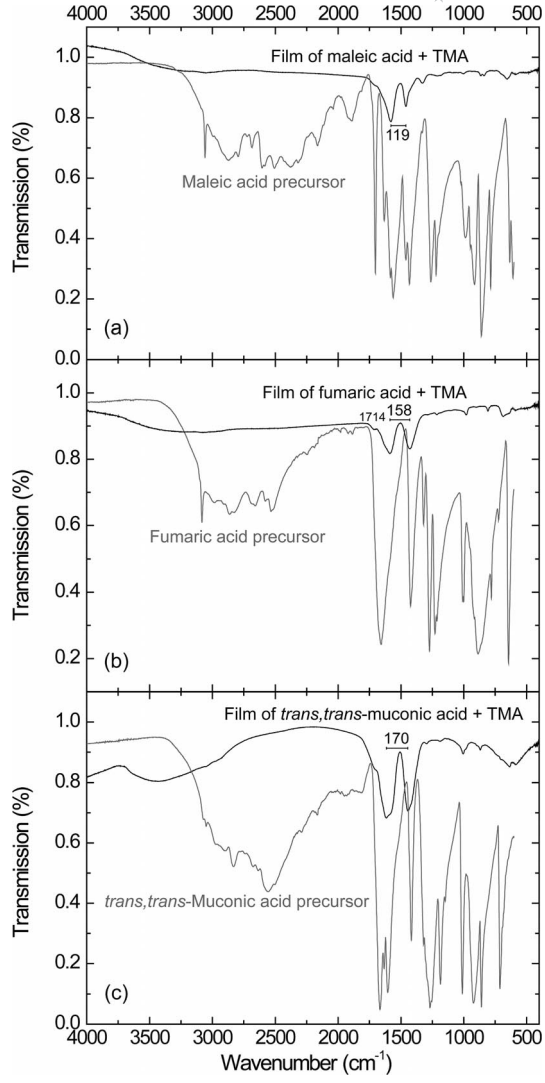

Figure 4. FTIR spectra of hybrid films of the unsaturated carboxylic acid/TMA systems and of the corresponding pure carboxylic acid precursors. The wave number splitting (cm^{-1}) between the asymmetric and symmetric carboxylate bands (Δ) are given.

Selected films were measured by FTIR spectroscopy and their absorption characteristics are shown in Figure 4. Absorption bands consistent with carboxylate groups, such as the asymmetric stretch around 1600 cm^{-1} and symmetric stretch just below 1500 cm^{-1}, are visible in all spectra.[18] The widths of the frequency splitting between these bands are included in the plots (Figure 4). A splitting between the asymmetric and symmetric carboxylate stretching bands (Δ) in the range 50–150 cm^{-1} is typical for bidentate complexes, unidentate complexes have $\Delta > 200\ cm^{-1}$, and bridging complexes have Δ in the range 130–200 cm^{-1}.[19]

Based on these guidelines, the interactions of the maleic acid/TMA system seem to be of a bidentate type, while the *trans,trans*-muconic acid/TMA system shows the formation of a complex of the bridging type. The frequency splitting of the fumaric acid/TMA system indicates a preference for the formation of a bridging type of complex as opposed to a bidentate type of complex. The transformation from *cis*- to *trans* configuration between maleic and fumaric acid seems to influence the type of bonding configuration that is formed in the films, as in all other respects the precursor acids are the same. The broad absorption bands that are observable in the 3700–2800 cm^{-1} regions of the spectra for all films are due to the presence of OH groups.[18] Such broadening of the very intense OH bands is quite typical in spectra of solid compounds.

The band associated with the asymmetric carboxylate stretch is broader in the spectrum for the *trans,trans*-muconic acid/TMA system than those observed in the spectra for the other two systems presented in Figure 4. This can be related to the two double bonds in the *trans,trans*-muconic acid molecule. The conjugated alkene double bond may have asymmetric and symmetric stretches at around 1650 and 1600 cm^{-1}, respectively. The absorption frequency of an alkene double bond in conjugation with a carbonyl group is lower by about 30 cm^{-1}.[18] The intensity of the absorption is markedly increased compared to that of a single double bond stretch. As the *trans,trans*-muconic acid molecule is symmetrical, only the asymmetric double bond stretch would be visible in its IR spectrum. This band could

in turn be superimposed on the asymmetric stretching band of the carboxylate group, rendering the total observed band quite broad. For clarification, the spectra of powders of the pure carboxylic acids used as precursors in this study are included, for reference, in Figure 4.

The presence of aluminium in the deposited films was verified by X-ray fluorescence (XRF) measurements. Some possible reaction intermediates and bonding schemes between the carboxylic acids and aluminium cations are given in Figure 5.

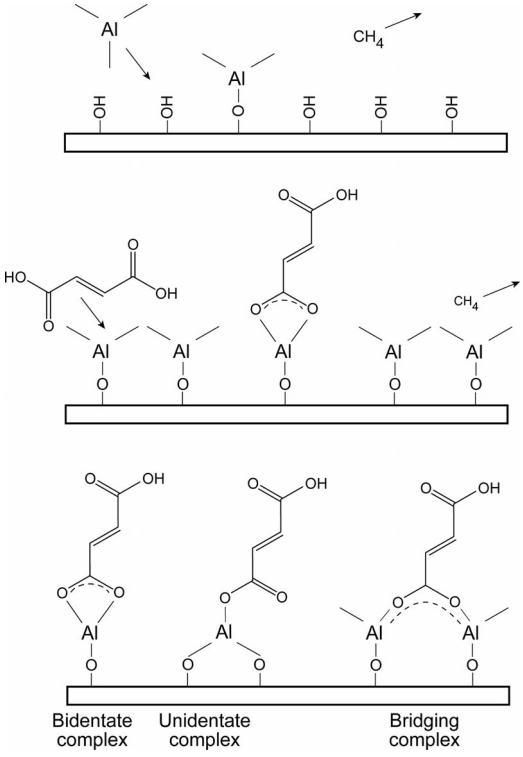

Figure 5. Illustration of possible reaction mechanisms and resulting bonding situations arising from the deposition process.

X-ray diffraction analyses indicate an amorphous character of the as-deposited films, Figure 6. This finding was concluded from both standard θ–2θ diffraction and gracing incidence XRD (GIXRD) measurements.

Most films exhibit quite low surface roughness as measured by AFM, typically in the range 0.2–1.3 nm (Figure 7), with the exception of the film of the maleic acid/TMA system deposited at 138 °C (12.7 nm). A low surface roughness is a typical property of thin films of amorphous materials.

Surface topographies, as measured by AFM, are shown for selected systems in Figure 8. The films were deposited on Si(111) at temperatures in the range 138–300 °C and were investigated as deposited. The most distinct topography is found for the maleic acid/TMA system deposited at 138 °C, which exhibits surface features of around 110 nm in width, Figure 8a. However, the film of the same system deposited at 186 °C shows almost no distinct surface features, Figure 8b. The films of the fumaric acid/TMA and *trans*,*trans*-muconic acid/TMA systems display quite smooth surfaces with little surface distinction.

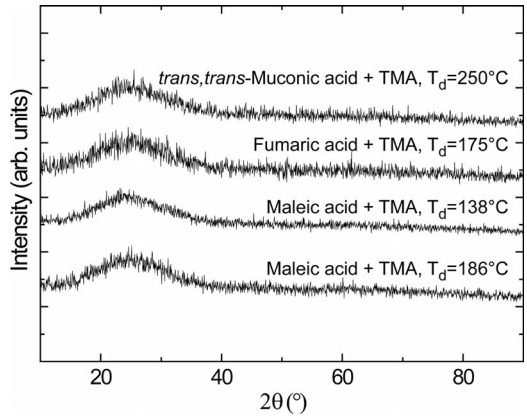

Figure 6. θ–2θ Diffractograms for the as-deposited films of the maleic acid/TMA, fumaric acid/TMA, and *trans*,*trans*-muconic acid/TMA systems on soda-lime glass.

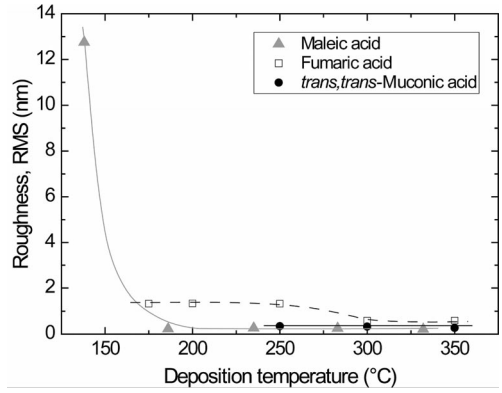

Figure 7. Surface roughness (root-mean-square, RMS) as a function of deposition temperature for the carboxylic acid/TMA systems. The films were deposited during 60 cycles, apart from the maleic acid/TMA system for which 150 cycles were used. The film thicknesses are in the range 35–117 nm.

All films appear stable in air and do not exhibit any measurable changes in thickness, as measured by XRR, or in transparency or in colour as observed visually, or in FTIR characteristics, after being exposed to air for one week and for one year.

Some physical properties of the films were screened by determination of their contact angles with water, and by UV/Vis spectroscopy and ellipsometry measurements. Contact angles between the droplets of water and the films are given in Table 2. For comparison, contact angles for an aluminium oxide film and for a silicon substrate with a native SiO_x layer were also measured (Table 2). The aluminium oxide film represents the inorganic counterpart of the deposited hybrid films. The amorphous SiO_x layer represents the starting point before deposition of the film. The contact angle is measured on the inside of the water droplet, and the tangent is calculated analytically by a circular curve fit of the profile points that are closest to the baseline. This is illustrated for the *trans*,*trans*-muconic acid/TMA system in Figure 9.

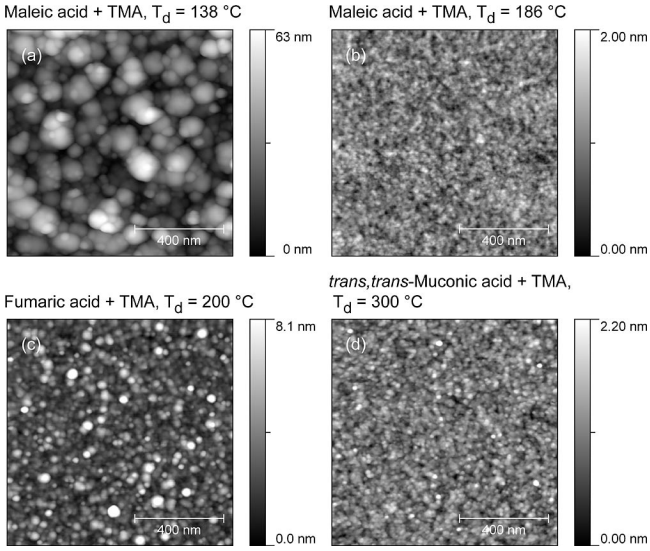

Figure 8. Topography, as measured by AFM, of films deposited on Si(111). The films are based on TMA and (a) maleic acid (T_d = 138 °C, thickness ≈ 116 nm), (b) maleic acid (T_d = 186 °C, thickness ≈ 81 nm), (c) fumaric acid (T_d = 200 °C, thickness ≈ 64 nm), (d) *trans*,*trans*-muconic acid (T_d = 300 °C, thickness ≈ 53 nm).

Table 2. Contact angle data for the organic–inorganic films and reference materials.

Thin film system	Contact angle [°] (ESD ≤ 0.1°)
Maleic acid/TMA	93.8
Fumaric acid/TMA	92.3
trans,*trans*-Muconic acid/TMA	96.5
Al_2O_3	95.6
Si(111) substrate	155.2

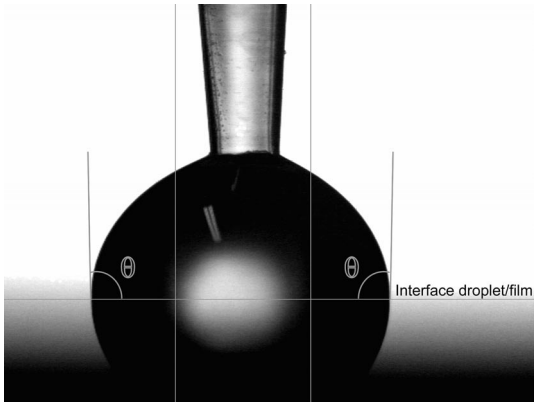

Figure 9. Contact angle between water and the *trans*,*trans*-muconic acid/TMA thin film. The horizontal line indicates the interface between the water droplet and the film surface.

UV/Vis transmission measurements of the films deposited on thin soda-lime glass substrates proved that the maleic acid/TMA and fumaric acid/TMA systems are transparent in the range 200–1700 nm, whereas the *trans*,*trans*-muconic acid/TMA system showed a slight absorbance for wavelengths below 470 nm, Figure 10. The refractive indices were calculated from a Cauchy fit of the ellipsometry data, see inset in Figure 10. The Cauchy fit was chosen as it uses a minimum of parameters (thickness and refractive index) adaptable for transparent films in the measured range. The slight absorbance of the *trans*,*trans*-muconic acid/TMA system resulted in difficulties in obtaining a reasonable Cauchy fit to the data at wavelengths lower than 470 nm (inset Figure 10). No improvement was achieved by using other fit functions.

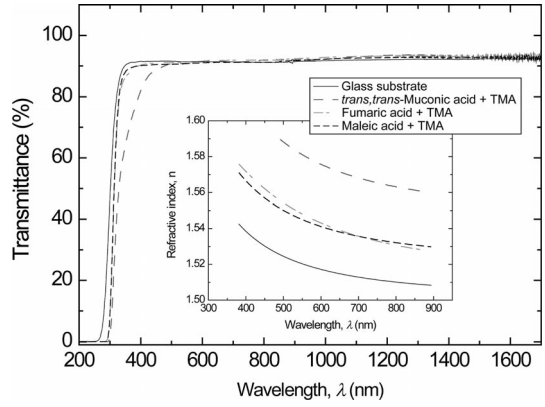

Figure 10. UV/Vis transmission characteristics as a function of wavelength of the as-deposited films on thin soda-lime glass substrates. Data for the clean glass substrate is included. Refractive indices as a function of wavelength are shown in the inset.

Growth Rates

The QCM investigations show self-hindered growth for all systems (Figure 1). In the case of the fumaric acid/TMA and *trans*,*trans*-muconic acid/TMA systems, the observed delay period suggests either a slow reaction of the precursors or, more likely, a delayed transport of the acid precursor to the substrate. This matter has not been a subject of this investigation.

The QCM data can also be used to extract information on possible reaction schemes by comparing the relative mass increase from the different pulses with a suitable model. All three acids presented in this work are bifunctional and should, for a stoichiometric reaction, follow the path:

Step 1 with the introduction of TMA:

$$|\text{–(OH)}_x + \text{Al(CH}_3)_3\text{(g)} \rightarrow |\text{–O}_x\text{–Al–(CH}_3)_{3-x} + x\text{CH}_4\text{(g)}\ \Delta m_1$$

Step 2 with the introduction of the acid:

$$|\text{–O}_x\text{–Al–(CH}_3)_{3-x} + 1.5\ R\text{-C}_2\text{O}_4\text{H}_2 \rightarrow |\text{–O}_x\text{–Al–}(R\text{-C}_2\text{O}_4\text{H}_{(2/3x)})_{1.5} + (3 - x)\text{CH}_4\text{(g)}\ \Delta m_2$$

where R = C_2H_2 for maleic acid and fumaric acid, and R = C_4H_4 for *trans*,*trans*-muconic acid.

The observed relative mass changes ($\Delta m_1/\Delta m_2$) for these systems are 0.386, 1.25, and 0.705 for the maleic acid/TMA, fumaric acid/TMA and *trans*,*trans*-muconic acids/TMA systems, respectively. By fitting the stoichiometric reaction scheme given above with these observed mass changes, x values of 1.1, –2.4, and –1.6 can be obtained, respectively. The obtained x value for the maleic acid/TMA system is close to 1, indicating that only one of the methyl groups of the TMA molecule is able to react with the surface upon

introduction. This also indicates that when maleic acid is introduced to the surface, 2/3 of the available carboxylic acid groups involved in step 2 will undergo reaction with the methyl groups on the surface. This can be visualized by only one carboxylic acid group of each maleic acid molecule taking part in the reaction with the surface. However, for the stoichiometry to be upheld (Al:acid, 1:1.5), one acid molecule needs to be shared between two aluminium cations for every three acid molecules introduced to the surface. This leaves one acid molecule per aluminium cation free to react in the following reaction cycle (Figure 11). A cyclic arrangement of both acid groups of the maleic acid onto the same aluminium cation would probably be too constrained, particularly if a bidentate reaction mode of both the carboxylic acid groups should be upheld. Furthermore, this would prevent further growth of the film, unless only a small, constant fraction of the acid molecules underwent such a reaction.

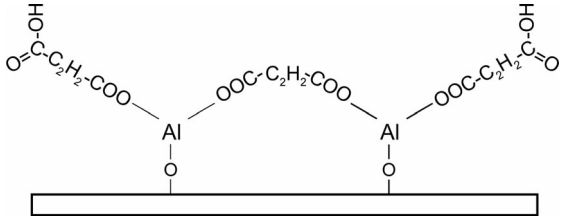

Figure 11. Proposed stoichiometric reaction scheme for the maleic acid/TMA system.

The *x* values obtained for the other two carboxylic acid/TMA systems are both outside the logical limits for the suggested reaction model. Both values are significantly negative, indicating that the mass increase during the TMA pulse is too high or that the mass increase during the introduction of the carboxylic acid is too low. When comparing the absolute mass increase during the TMA pulse for the different systems, it becomes evident that this mass increase is notably higher for the fumaric acid/TMA and *trans*,*trans*-muconic acids/TMA systems than for the maleic acid/TMA system. Such an excess mass increase during the TMA pulse may be a result of physical absorption of TMA into the film material during this pulse or that a significant fraction of the methyl groups remain unreacted during film growth. The reduction in mass during the purge after the TMA pulse is insignificant for all systems, indicating that any excess TMA must be bonded relatively strongly within the film.

In general, the reduction in growth rates at higher deposition temperatures (Figure 2) may be due to increased molecular thermal motions that overcome the weak interactions between the organic chains, which results in an increase in the steric hindrance at the surface as the temperature is increased, and thereby in the lowering of the number of available functional sites. At increased deposition temperatures, faster desorption of the chemisorbed precursor molecules may also occur, which contribute to the reduction in growth rate. The density of the deposited films is, on average, relatively constant throughout the ALD window and is approximately 2 $g cm^{-3}$ for all systems (Figure 3). This indicates that the material does not alter its overall amorphous structure within the temperature range investigated. The magnitude of the growth rates may be explained by the length of a single layer of acid molecules deposited during each cycle, when allowing for some stretching, reorganization and the rather vertical positioning of the acid molecules within the layer. However, the possibility of oligomerization cannot be ignored completely.

Topography

It is puzzling that the maleic acid/TMA system has rather large surface features that are observable in the topography image and, consequently, has a high surface roughness (12.7 nm RMS) and a slightly elevated density when compared to the other samples, yet, the XRD data show no sign of any crystalline phase in the film (cf. Figures 8a, 3 and 6). At higher deposition temperatures, the same system shows no sign of larger surface features, and the surfaces are very smooth (Figures 7 and 8). The QCM results provide no indication of inadequate purging of either TMA or maleic acid, the growth rates have no abrupt changes as function of deposition temperature, and there are no large gradients, which could indicate CVD growth or any signs of unreacted precursor acid in the FTIR data.

Structure

The FTIR spectra indicate that there are minor amounts of OH groups in the resulting film materials, although a slightly higher number of OH groups are present in the *trans*,*trans*-muconic acid/TMA system relative to the other materials. The OH bond absorbs strongly in the IR range, and hence this technique is sensitive for the detection of such groups. The low intensity of the signal from the OH groups and the remaining signal from the carboxylate groups in the spectra of the resulting materials therefore indicate that most of the OH groups within the carboxylic acid groups have undergone reactions with the TMA precursor. The rather weak OH bands could possibly indicate the presence of some absorbed water in the films upon exposure to air, which is not desorbed completely under the vacuum conditions of the FTIR instrument.

The difference in the *cis* and *trans* configurations of maleic and fumaric acid, respectively, appears to influence the bonding situation upon their reaction with TMA. The *trans* compound induces a higher growth rate and yields films with a higher surface roughness but with a lower density relative to the films generated with the *cis* compound. However, there are no differences with respect to the contact angles of the films with water, in the UV/Vis absorbance properties, or in the refractive index of the films prepared with these two acids.

Physical Properties

The degree of hydrophobicity of the *trans*,*trans*-muconic acid/TMA thin films appears to be elevated slightly relative

to those of the maleic acid/TMA and fumaric acid/TMA systems. The acid precursor is deposited as the terminating layer in the deposition process. The *trans,trans*-muconic acid has a longer carbon backbone (C = 6) relative to the other two systems (C = 4). The longer carbon backbone introduces more hydrophobic groups to the surface, and therefore the resulting film surface is slightly more hydrophobic. Given the rigidness of the backbone due to the conjugated double bonds, the possibility of double reactions of the *trans,trans*-muconic acid molecule should be restricted. However, if such a reaction should take place, this would leave the hydrophobic backbone of the acid facing outwards from the surface, and the hydrophobic character would naturally be greater.

The slight absorbance observed for wavelengths below 470 nm in the UV/Vis spectrum of the *trans,trans*-muconic acid/TMA system is also reflected in the increased refractive index of this system relative to those of the other two systems presented (Figure 10). The difficulties experienced in obtaining Cauchy fits for the data for this system are due to this slight absorbance, and may often be related to structural ordering within the system. No global ordering of the system is observed by XRD, but the increased rigidness of the organic molecule due to the conjugated double bonds may lead to an increase in the local ordering, which affects the total absorption of the system.

Conclusions

Thin films of organic–inorganic hybrid materials were successfully grown with unsaturated linear carboxylic acids and TMA. The influence of the *cis*- and *trans* configurations of the precursors was explored. The QCM measurements indicate self-limiting growth dynamics for the films, although the growth rates decrease as the deposition temperature increases. The films are generally X-ray amorphous, smooth, stable in contact with water, transparent, and have refractive index in the range 1.5–1.6.

Experimental Section

Thin films were deposited in an F-120 Sat reactor (ASM Microchemistry Ltd.) with TMA and the relevant unsaturated, linear carboxylic acid [maleic acid (Fluka, ≥99.0%), fumaric acid (Fluka, ≥99.5%) and *trans,trans*-muconic acid (Aldrich, ≥98%)] as precursors (Figure 12).

During deposition, a background pressure of ca. 3 mbar was obtained by applying a flow of N_2 carrier gas at a rate of 300 $cm^3 min^{-1}$. The gas was produced in a Schmidlin UHPN3001 N_2 purifier unit, with a claimed purity of 99.999% with respect to N_2 and Ar content.

The films were deposited on soda-lime glass and single crystal Si(111) substrates. The Si(111) substrates were used as obtained from the manufacturer, whereas the soda-lime glass substrates were cleaned with ethanol prior to use.

The film growth dynamics were examined by means of quartz crystal microbalance measurements with a Maxtek TM400 unit

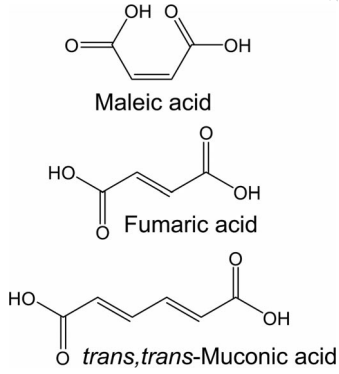

Figure 12. Organic precursors utilized in this work.

equipped with homemade crystal holders. In order to increase the accuracy of the QCM measurements, the data were post-processed by averaging data from 16 successive deposition cycles.

The growth was studied as a function of deposition temperature in the relevant deposition ranges for the various organic precursors. The overall temperature range covered was 138–332 °C.

The crystallinity of the films was examined by X-ray diffraction (XRD) with a Siemens D5000 diffractometer equipped with a Göbel-mirror that provided Cu-K_α radiation. This setup was used to measure X-ray reflectivity (XRR), grazing incidence X-ray diffraction (GIXRD), and conventional θ–2θ diffraction in reflection mode.

X-ray fluorescence (XRF) was used to determine the aluminium content in the films. The measurements were performed on a Philips PW2400, and the measured XRF intensities were analyzed with the UniQuant software.[20]

The topographies of representative sections of the films were studied with tapping atomic force microscopy (AFM) by using a Dimension 3100 instrument with a Nanoscope IIIa controller and NSC35/AlBS Si 10-nm tips that were obtained from Micromasch.

Selected as-deposited films on Si(100) were analyzed in vacuo (3 mbar) by Fourier transform infrared (FTIR) transmission spectroscopy with a Bruker IFS 66 VS spectrometer. An uncoated Si(111) substrate was used as reference. Powder samples of the carboxylic acids used as precursors were also measured, for reference, with a Perkin–Elmer Spectrum 2000 Explorer FTIR spectrometer with a single reflection diamond ATR and a DuraSamplIR II accessory supplied by SensIR Technologies.

Contact angle measurements were performed with the DROPimage analysis program (standard edition) version 2.4 and a ramé-hart Contact Angle Goniometer.

UV/Vis transmission measurements were performed with a Shimadzu UV-3600 instrument. The refractive indices were calculated on the basis of measurements made with an alpha-SE spectroscopy ellipsometer from J. A. Woollam; the data were fitted with a Cauchy function.

Acknowledgments

This work has received financial support from the FUNMAT@UiO effort and the Centre for Materials Science and Nanotechnology, University of Oslo, Norway. The authors are indebted to Professor Claus Jørgen Nielsen (University of Oslo) and Ingvil Gausemel (GE Healthcare) for help and discussions concerning FTIR

measurements, and Professor Finn Knut Hansen (University of Oslo) for aid with the contact angle measurements.

[1] R. J. Kuppler, D. J. Timmons, Q. R. Fang, J. R. Li, T. A. Makal, M. D. Young, D. Q. Yuan, D. Zhao, W. J. Zhuang, H. C. Zhou, *Coord. Chem. Rev.* **2009**, *253*, 3042–3066.

[2] D. Zacher, O. Shekhah, C. Woll, R. A. Fischer, *Chem. Soc. Rev.* **2009**, *38*, 1418–1429.

[3] a) S. M. George, *Chem. Rev.* **2010**, *110*, 111–131; b) R. L. Puurunen, *J. Appl. Phys.* **2005**, *97*, 121301; c) M. Ritala, M. Leskelä in *Handbook of Thin Film Materials*, Vol. 1 (Ed.: H. S. Nalwa), Academic Press, San Diego CA, **2002**, pp. 103–159.

[4] a) N. M. Adarnczyk, A. A. Dameron, S. M. George, *Langmuir* **2008**, *24*, 2081–2089; b) I. S. Bae, S. J. Cho, W. S. Choi, B. Y. Hong, Y. J. Kim, Y. M. Kim, J. H. Boo, *Thin Solid Films* **2008**, *516*, 3577–3581; c) R. C. Chambers, E. J. Osburn Atkinson, D. McAdams, E. J. Hayden, D. J. Ankeny Brown, *Chem. Commun.* **2003**, 2456–2457; d) C.-C. Chang, W.-C. Chen, *Chem. Mater.* **2002**, *14*, 4242–4248; e) G. Gu, Z. Zhang, H. Dang, *Mater. Res. Bull.* **2004**, *39*, 1037–1044; f) G. Gu, Z. Zhang, H. Dang, *Appl. Surf. Sci.* **2004**, *221*, 129–135; g) A. Kobayashi, H. Naito, Y. Matsuura, K. Matsukawa, S. Nihonyanagi, Y. Kanemitsu, *J. Non-Cryst. Solids* **2002**, *299–302*, 1052–1056; h) B. H. Lee, K. H. Lee, S. Im, M. M. Sung, *J. Nanosci. Nanotechnol.* **2009**, *9*, 6962–6967; i) R. Makote, M. M. Collinson, *Chem. Mater.* **1998**, *10*, 2440–2445; j) F. Mammeri, L. Rozes, C. Sanchez, E. Le Bourhis, *J. Sol-Gel Sci. Technol.* **2003**, *26*, 413–417; k) M. Minelli, M. G. De Angelis, F. Doghieri, M. Marini, M. Toselli, F. Pilati, *Eur. Polym. J.* **2008**, *44*, 2581–2588; l) N. Umeda, A. Shimojima, K. Kuroda, *J. Organomet. Chem.* **2003**, *686*, 223–227.

[5] M. N. Antipina, R. V. Gainutdinov, I. V. Golubeva, Y. A. Koksharov, A. P. Malakho, S. N. Polyakov, A. L. Tolstikhina, T. V. Yurova, G. B. Khomutov, *Surf. Sci.* **2003**, *532–535*, 1017–1024.

[6] a) A. A. Dameron, D. Seghete, B. B. Burton, S. D. Davidson, A. S. Cavanagh, J. A. Bertrand, S. M. George, *Chem. Mater.* **2008**, *20*, 3315–3326; b) S. M. George, B. Yoon, A. A. Dameron, *Acc. Chem. Res.* **2009**, *42*, 498–508; c) K. B. Klepper, O. Nilsen, H. Fjellvag, *Dalton Trans.* **2010**, *39*, 11628–11635; d) K. B. Klepper, O. Nilsen, H. Fjellvåg, at *Baltic Conference on Atomic Layer Deposition*, Oslo, Norway, **2006**; e) K. B. Klepper, O. Nilsen, H. Fjellvåg, at *E-MRS 2007 Fall Meeting*, Warsaw, Poland, **2007**; f) K. B. Klepper, O. Nilsen, H. Fjellvåg, at *7th International Conference on Atomic Layer Deposition*, San Diego, California, USA, **2007**; g) K. B. Klepper, O. Nilsen, H. Fjellvåg, at *8th International Conference on Atomic Layer Deposition*, Bruges, Belgium, **2008**; h) K. B. Klepper, O. Nilsen, H. Fjellvåg, at *Baltic Conference on Atomic Layer Deposition*, Uppsala, Sweden, **2009**; i) K. B. Klepper, O. Nilsen, H. Fjellvåg, at *9th International Conference on Atomic Layer Deposition*, Monterey, CA, USA, **2009**; j) K. B. Klepper, O. Nilsen, P.-A. Hansen, H. Fjellvag, *Dalton Trans.* **2011**, *40*, 4636–4646; k) X. Liang, D. M. King, P. Li, S. M. George, A. W. Weimer, *AIChE J.* **2009**, *55*, 1030–1039; l) O. Nilsen, H. Fjellvåg [Ed.: W. I. P. O. Patent Cooperation Treaty (PCT)], **2006**, p. 42; m) O. Nilsen, K. B. Klepper, H. Ø. Nielsen, H. Fjellvåg, *ECS Trans.* **2008**, *16*, 3–14; n) Q. Peng, B. Gong, R. M. VanGundy, G. N. Parsons, *Chem. Mater.* **2009**, *21*, 820–830; o) B. Yoon, J. L. O'Patchen, D. Seghete, A. S. Cavanagh, S. M. George, *Chem. Vapor Depos.* **2009**, *15*, 112–121; p) B. Yoon, D. Seghete, A. S. Cavanagh, S. M. George, *Chem. Mater.* **2009**, *21*, 5365–5374.

[7] a) K. Chondroudis, D. B. Mitzi, *Chem. Mater.* **1999**, *11*, 3028–3030; b) D. B. Mitzi, K. Chondroudis, C. R. Kagan, *Inorg. Chem.* **1999**, *38*, 6246–6256; c) D. B. Mitzi, M. T. Prikas, K. Chondroudis, *Chem. Mater.* **1999**, *11*, 542–544.

[8] Z. Y. Cheng, H. F. Wang, Z. W. Quan, C. K. Lin, J. Lin, Y. C. Han, *J. Cryst. Growth* **2005**, *285*, 352–357.

[9] a) D. Bersani, P. P. Lottici, M. Casalboni, P. Prosposito, *Mater. Lett.* **2001**, *51*, 208–212; b) M. Era, S. Morimoto, T. Tsutsui, S. Saito, *Appl. Phys. Lett.* **1994**, *65*, 676–678; c) H. Han, J. Bissell, F. Yaghmaie, C. E. Davis, *Langmuir* **2010**, *26*, 515–520; d) C. R. Kagan, D. B. Mitzi, C. D. Dimitrakopoulos, *Science* **1999**, *286*, 945–947; e) Y. H. Li, H. J. Zhang, S. B. Wang, Q. G. Meng, H. R. Li, X. H. Chuai, *Thin Solid Films* **2001**, *385*, 205–208; f) D. B. Mitzi, C. D. Dimitrakopoulos, L. L. Kosbar, *Chem. Mater.* **2001**, *13*, 3728–3740; g) Z.-L. Xiao, H.-Z. Chen, M.-M. Shi, G. Wu, R.-J. Zhou, Z.-S. Yang, M. Wang, B.-Z. Tang, *Mater. Sci. Eng. B* **2005**, *117*, 313–316.

[10] a) L. Li, M. Mizuhata, S. Deki, *Appl. Surf. Sci.* **2005**, *239*, 292–301; b) R. Martins, R. Silva, R. Gonçalves, O. Serra, *J. Fluoresc.* **2010**, *20*, 739–743; c) E. J. Nassar, R. R. Gonçalves, M. Ferrari, Y. Messaddeq, S. J. L. Ribeiro, *J. Alloys Compd.* **2002**, *344*, 221–225.

[11] R. Houbertz, G. Domann, C. Cronauer, A. Schmitt, H. Martin, J. U. Park, L. Fröhlich, R. Buestrich, M. Popall, U. Streppel, P. Dannberg, C. Wächter, A. Bräuer, *Thin Solid Films* **2003**, *442*, 194–200.

[12] K. H. Haas, S. Amberg-Schwab, K. Rose, G. Schottner, *Surf. Coat. Technol.* **1999**, *111*, 72–79.

[13] G. Cao, M. E. Garcia, M. Alcala, L. F. Burgess, T. E. Mallouk, *J. Am. Chem. Soc.* **1992**, *114*, 7574–7575.

[14] J. A. de Saja, M. L. Rodriguez-Mendez, *Adv. Colloid Interface Sci.* **2005**, *116*, 1–11.

[15] B. Darracq, F. Chaput, K. Lahlil, J.-P. Boilot, Y. Levy, V. Alain, L. Ventelon, M. Blanchard-Desce, *Opt. Mater.* **1998**, *9*, 265–270.

[16] D. C. Miller, R. R. Foster, S. H. Jen, J. A. Bertrand, D. Seghete, B. Yoon, Y. C. Lee, S. M. George, M. L. Dunn, *Acta Materialia* **2009**, *57*, 5083–5092.

[17] G. Sauerbrey, *Z. Phys.* **1959**, *155*, 206–222.

[18] a) R. M. Silverstein, F. X. Webster, D. J. Kiemle in *Spectrometric Identification of Organic Compounds*, 7th ed. (Ed.: S. Wolfman-Robichaud), John Wiley & Sons Inc., Hoboken, NJ, **2005**, pp. 72–126; b) H. F. Shurvell in *Handbook of Vibrational Spectroscopy – Sample Characterisation and Spectral Data processing*, Vol. 3 (Eds.: J. M. Chalmers, P. R. Griffiths), John Wiley & Sons Ltd., Chichester, UK, **2002**, pp. 1783–1816.

[19] F. Verpoort, T. Haemers, P. Roose, J. P. Maes, *Appl. Spectrosc.* **1999**, *53*, 1528–1534.

[20] *Neptunus 2*, 2nd ed., Omega Data Systems, NL-5505 Veldhoven, The Netherlands, **1994**.

Received: February 24, 2011
Published Online: November 2, 2011

